Real-Time Quantum Dynamics of Interacting Electrons: Self-Organized Nanoscale Structure in a Spin-Electron Coupled System

W. Koshibae,[1] N. Furukawa,[2,3] and N. Nagaosa[1,4]

[1]*Cross-Correlated Materials Research Group (CMRG), RIKEN, Saitama 351-0198, Japan*
[2]*Aoyama-Gakuin University, 5-10-1, Fuchinobe, Sagamihara, Kanagawa 229-8558, Japan*
[3]*ERATO-Multiferroics, JST, c/o Department of Applied Physics, The University of Tokyo, Tokyo 113-8656, Japan*
[4]*Department of Applied Physics, The University of Tokyo, Tokyo 113-8656, Japan*

(Received 3 May 2009; published 28 December 2009)

We investigate the quantum evolution of the excited electronic states combined with the classical dynamics of the order parameter field in a spin-electron coupled system. It is found that the nanoscale spatial structure of the spins evolves spontaneously accompanied by the localization of the electronic wave functions, and the nonadiabatic quantum transitions through a resonant mutual precession analogous to the electron spin resonance (ESR) process.

DOI: 10.1103/PhysRevLett.103.266402 PACS numbers: 71.10.Fd, 78.20.Bh

The cross effect between electronic transport and external field is fundamental to electronics, and is nothing more than the control of the excitation and its relaxation dynamics by the external field. In a bid for faster and higher sensitive electronic devices beyond the conventional semiconductors which physics is well described by the single carrier problem, the phase control of the strongly interacting electron systems has attracted much attention. The colossal magnetoresistance is an example of the control of the spin, charge, and orbital ordering by external fields [1], where the nanoscale structures play essential roles [2]. One of the most urgent and vital issues today is the real-time dynamics of interacting electrons, a typical example of which is the relaxation after the photoexcitations [3–7]. In the semiconductors, the relaxation dynamics of the excited states is governed by the lattice degree of freedom, i.e., the excited electrons show its relaxation via coupling to the phonons. On the other hand, in the strongly interacting electron systems, there exists another degree of freedom acting on the highly nontrivial relaxation dynamics, that is, the spins. In more general cases, the dynamics of the interacting electrons can be translated into the motion of the *noninteracting* electrons in the background of the fluctuating *spin field* [1]. Therefore, the relaxation dynamics of the spin-electron coupled system is one of the most fundamental issues in this research field.

In this Letter, we study the relaxation dynamics of the excited states in the system, where the classical spins are coupled to the conduction electrons. We find that the self-organized space-time structure of the spins and electrons is formed spontaneously through the quantum transition analogous to the electron spin resonance (ESR) process with the fluctuating spin field. In particular, in the magnetically ordered states, the coupled equations of motion for the classical spins and quantum electrons can describe the dynamics of the interacting electrons because the order parameter behaves as a classical field [8]. This method enables us to study the space-time structure of the quantum dynamics, and also to obtain the intuitive physical picture in larger-size or higher-dimensional systems for longer time period. Therefore, the present work is complementary to the previous ones for fully quantum systems [9–11] where the system size or time period are limited.

We start with the Hamiltonian [12] on the square lattice,

$$\hat{H} = -t\sum_{\langle ij\rangle,s} c_{is}^{\dagger}c_{js} + \text{H.c.} - J_H\sum_{iss'} c_{is}^{\dagger}c_{is'}\vec{\sigma}_{ss'}\cdot\vec{S}_i, \quad (1)$$

where $\langle ij\rangle$ denotes a nearest-neighbor pair, s and s' are indices for electron spin, respectively, and $\vec{\sigma}_{ss'}$ is given by Pauli matrices. The local spins, $\vec{S}_i$'s, are taken to be classical vectors with magnitude S. Other notations are standard. We consider the half-filled case.

Using finite size systems, we numerically investigate the time evolution of the electronic states and local spins. The equation of motion for the local spins is expressed by the Landau-Lifschitz-Gilbert (LLG) equation, $\dot{\vec{S}}_i = -J_H\langle\vec{\sigma}_i\rangle\times\vec{S}_i - \alpha\vec{S}_i\times\dot{\vec{S}}_i$, where $\langle\vec{\sigma}_i\rangle$ is the expectation value of electron spin at site i, and the Gilbert damping constant $S\alpha$ is introduced to include energy dissipation processes for spins. When $\langle\vec{\sigma}_i\rangle$ is fixed, the solution of the LLG equation is given by $\phi_i(T) = -[(SJ_H/t)|\langle\vec{\sigma}_i\rangle|/(1+(S\alpha)^2)](t/S)T$, and $\theta_i(T) = 2\tan^{-1}[\tan(\theta_{i0}/2)\exp(S\alpha\phi_i)]$, where (θ_i, ϕ_i) is the polar and azimuthal angles of $\vec{S}_i$ in the local-spin coordinate where z axis is parallel to $\langle\vec{\sigma}_i\rangle$ and initial value of ϕ_i is zero, and T is time. The initial value of θ_i is written by θ_{i0}. Evolution of the electronic state $|\Phi(T)\rangle$ is given by $|\Phi(T)\rangle = \hat{U}(T)|\Phi(0)\rangle$, where $\hat{U}(T)$ is a unitary operator for the time evolution. If $\{\vec{S}_i\}$ are fixed, we have $\hat{U}(T) = \exp(-i\hat{H}T)$. We successively calculate the evolution of the electronic state and the LLG equation for a small time increment ΔT to investigate evolutions of the system in total. The changes in $\{\vec{S}_i\}$ and $|\Phi(T)\rangle$ are reflected to the calculation through $\hat{H}$ and $\{\langle\vec{\sigma}_i\rangle\}$.

The Hamiltonian (1) is expressed by a bilinear form of fermion operators. In such a case, we restrict ourselves to initial states which are given by single Slater determinant states constructed by N products of single-particle states $\phi_j(0)$. Then, it is known that time-evolved states are given by products of time-evolved single-particle states $\phi_j(T)$ which remain within the single Slater determinant states [13]. Note that $\phi_j(T)$'s are different from the eigenstates of the Hamiltonian (1) at each time T. This implies that our formalism is in sharp contrast with an adiabatic approximation where states are determined by occupying energy eigenstates at each time T.

Figure 1 shows the calculated result on the system of size 8×8 with the periodic boundary condition and a parameter set, $t = 1$, $SJ_H = 2$, $S\alpha = 1$, $S = 1$, $\Delta T = 0.008$. The lower panel of Fig. 1(a) is the time (T) dependence of the energy level structure. The Fermi level is taken to be zero. At around $T \sim 0$, we clearly see the energy gap $2SJ_H$ between upper and lower energy bands in the lower panel of Fig. 1(a). We prepare the initial state in the following way: The ground state of the model (1) at half filling is the antiferromagnetic (AFM) insulating state because of the perfect nesting condition in this system. In order to mimic the thermal fluctuation, we introduce a random tilting of each spin from the AFM configuration up to 0.1 rad which corresponds to the state with an excitation energy of $\sim 0.001t$ from the ground state. For the initial state, we fill up the lower energy band, and then transfer two electrons from the lowest eigenstates in the lower energy band to the two highest levels in the upper energy band. In the upper panel of Fig. 1(a), the number of electron of the *highest* (*lowest*) energy states in the upper energy band is shown by the broken (dotted) line, and the solid line is the number of electron in the upper energy band. Figures 1(b)–1(e) show the time dependence of the configuration of the local spins, while Figs. 1(f)–1(i) are the corresponding local energy density defined by the expectation value of $-(t/2)\sum_{\rho,s}(c^\dagger_{is}c_{\rho s} + \text{H.c.}) - J_H\sum_{ss'}c^\dagger_{is}c_{is'}\vec{\sigma}_{ss'}\cdot\vec{S}_i$, where ρ runs over the nearest-neighbor sites of i. In the Figs. 1(f)–1(i), the energy of the ground state is taken to be zero.

We find several distinct time regions, stages (I)–(III):

Stage (I): Self-organization process.—Even if we start with the almost perfect AFM spin configuration, the system develops spontaneously the spatial inhomogeneity with energy dissipation. At around $T = 20 \sim 40$, the electrons at the highest two energy states start to spread into lower energy states within the upper energy band [see the broken line in the upper panel of Figs. 1(a), 1(b), and 1(f)]. As shown in Fig. 1(f), the excitation energy is already localized well within the sample size. When we start with the more disordered spin configuration corresponding to the room temperature, the wave fuctions are localized as in Fig. 1(f) from the beginning, and the successive relaxation is essentially the same. Up to $T \sim 170$, the deviation of the spins are not so large moving around the original direction as shown by the snapshot in Fig. 1(c) at $T = 80$. This small amplitude spin fluctuation can induce the intraband transitions of the excited electrons to lower and lower energy state. The energy distribution shows the gentle spatial dependence with the reduced average as shown in Fig. 1(g) for $T = 80$. This means that the electronic wave functions are rather extended though slightly disturbed by the small tilting of the spins.

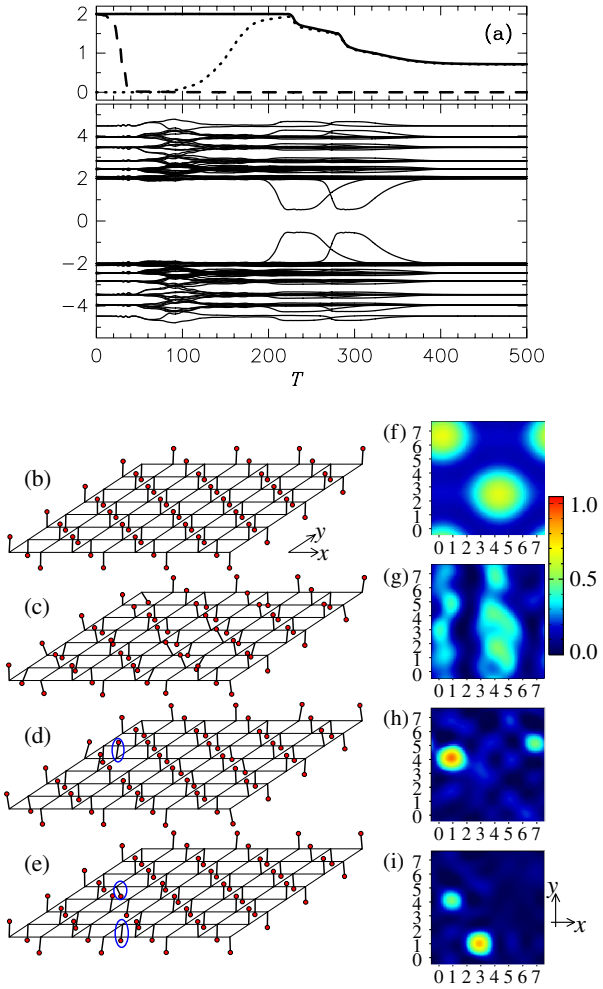

FIG. 1 (color online). Time evolution of the double-exchange model (see text). (a) The lower panel shows the time (T) dependence of the energy level structure. In the upper panel, the number of electrons in the upper energy band (solid line), in the *highest* two energy states (broken line), and in the *lowest* energy states of the upper energy band (dotted line) are shown. Configuration of local spins at $T = 28$, 80, 224, and 288 are presented in (b), (c), (d), and (e), respectively. Dot indicates the head of local spin. The local spins marked by ellipses in (d) and (e) are strongly deviated from the ground state. Figures (f), (g), (h) , and (i) show the distribution of excitation energy density measured from the ground state at $T = 28$, 80, 224, and 288, respectively. A spline interpolation is used for the contour maps.

Stage (II): Relaxation process with interband transition.—The inhomogeneity developed in the previous stage brings about a remarkable localization behavior and derives a dynamic relaxation process with the interband tran-

sition. At around $T \sim 220$, the electronic and local-spin structures show a dramatic change characterized by the large-amplitude motion of a local spin marked by an ellipse in Fig. 1(d). This motion starts at $T \sim 200$. At this time, the excited electrons reach the *lowest* states in the upper energy band as shown by the dotted line in the upper panel of Fig. 1(a), and find the localized place to relax furthermore. That is, the localization of the electronic state together with the large-amplitude local-spin motion with the polar angle of the order of π occurs concomitantly. This corresponds to a pair of the in-gap energy levels split off from the edge of the upper and lower energy bands at around $T \cong 200$, as seen in the lower panel of Fig. 1(a). When the separation of in-gap energy levels is smallest, the number of electrons in the upper energy band decreases rapidly [see the solid line in Fig. 1(a)]. After that, the local spin recovers toward its original direction, and the in-gap states merge again into the upper and lower energy bands. As shown in Fig. 1(h) for $T = 224$, the excitation energy is concentrated around this local spin, which in turn drives a motion of that local spin. In the same way, the relaxation dynamics with interband transition occurs again at $T \sim 300$, around another site [see Figs. 1(a), 1(e), and 1(i)]. This transition through the in-gap states reminds us of the Landau-Zener mechanism. However, a more thorough study given below reveals that it is a *resonant* transition and is completely different from the Landau-Zener process.

Stage (III): Relaxation process to a metastable state.— After $T \sim 400$, the active motion of the local spins is finished and the alignment becomes nearly perfect AFM. The excited electrons, however, remain more than ~ 0.7 in the upper energy band. This metastable state continues for a long time within our simulation (at least up to $T \sim 8000$).

Now we consider the quantum dynamics in more depth. As discussed below, there are two components of the local spins, i.e., the *rapid* oscillation and the *slow* motion as expressed by $\vec{S}_i = \vec{S}_i^{\text{slow}} + \vec{S}_i^{\text{rapid}}$. Let us first consider the *rapid* oscillation. Figure 2(a) shows the y component of the local spin moving with a largest deviation from the AFM ground state configuration through stage (I), and the inset is the trajectory of the local spin on the S_x-S_y plane. As seen in Fig. 2(a), the local spin shows an oscillation with a period of $T_p \cong 12$, i.e., the frequency $\omega (= 2\pi/T_p) \cong 0.5$. We find that this frequency ω corresponds to the difference of the energy between the highest (ε_1) and second highest (ε_2) energy levels in the lower panel of Fig. 1(a). The rapid oscillation $\vec{S}_i^{\text{rapid}}$ is driven by time dependence of $\vec{\sigma}$ in the LLG equation: when the wave function has the form $|\psi(t)\rangle = c_1(t)|1\rangle + c_2(t)|2\rangle$ with $c_a(t) = c_a(0)e^{-i\varepsilon_a t}$, $\langle\vec{\sigma}_i(t)\rangle$ has the component proportional to $c_1(t)^* c_2(t)\langle 1|\vec{\sigma}_i|2\rangle \propto e^{i(\varepsilon_1-\varepsilon_2)t}$ and its complex conjugate. Putting this into the LLG equation, we obtain $\vec{S}_i^{\text{rapid}}(t) \propto c_1(t)^* c_2(t)\langle 1|\vec{\sigma}_i|2\rangle \times \vec{S}_i^{\text{slow}} + \text{H.c.}$ This interpretation is consistent with the Fourier spectral weight [14] of the spin motion in Fig. 2(e), where the peak is observed around the frequency $\omega \cong 0.5$, which corresponds to $\varepsilon_1 - \varepsilon_2$ in stage (I). This *rapid* oscillation in turn induces the transition between the state $|1\rangle$ and $|2\rangle$, analogously to the ESR where the oscillating transverse magnetic field induces the Rabi oscillation. Figure 2(b) is the time dependence of the electron occupation number at the highest energy states at stage (I), and it clearly shows this Rabi oscillation with the frequency (Ω) determined by the oscillation amplitude (δS^{rapid}) of $\vec{S}_i^{\text{rapid}}$. From Fig. 2(a), we can read the oscillation amplitude $\delta S^{\text{rapid}} \cong 0.3$, so that the frequency Ω is estimated to be $J_H \delta S^{\text{rapid}} \cong 0.6$. Therefore, the occupation number will show an oscillation with a period of $2\pi/(2\Omega) \cong 5.2$. This oscillation is actually observed as shown in Fig. 2(b). With the Gilbert damping, this oscillation is the damped one and the occupation number of the lower energy state increases.

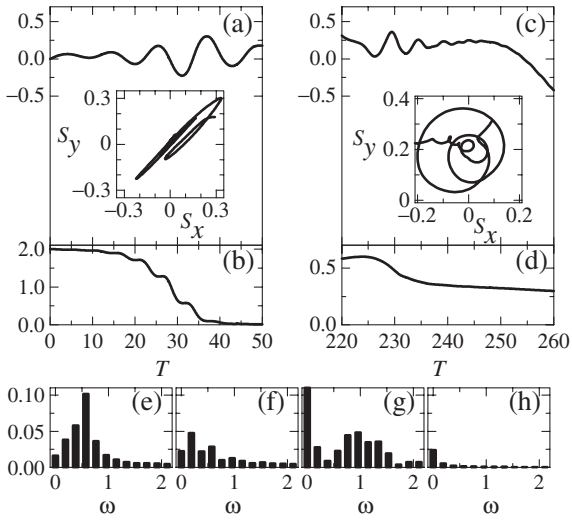

FIG. 2. Relaxation driven by *rapid* oscillation. (a) The y component of the local spin which shows the largest deviation from the AFM ground state configuration in stage (I). The inset is the trajectory of the local spin on the S_x-S_y plane. (b) The electron occupation number at the highest energy states. (c) The same with (a) but in stage (II). (d) The electron occupation number at the lowest energy state (in-gap state) in the upper energy band. (e) The Fourier spectral weight of (a). (f) The same with (e) but $T = 132$. (g) The Fourier spectral weight of (c). (h) The same with (f) but $T = 600$.

With the time evolution at stage (I), the excited electrons are distributed into lower energy levels, so that the spatial inhomogeneity appears as observed in the spatial distribution of the local energy density. The inhomogeneity has also been observed in the spatial distribution of the magnitude of electron spins. Reflecting the inhomogeneity, the magnitude of the *rapid* oscillation of the local spin depends on the sites in real space strongly. When we look at the local spins at other sites, this *rapid* oscillation is almost missing and only the slow and small amplitude motion is observed. This means that the site-selective lock-in of the *rapid* oscillation of the spins occurs self-consistently with the electronic levels before and after the transitions. This self-organized space-time structure is the most basic

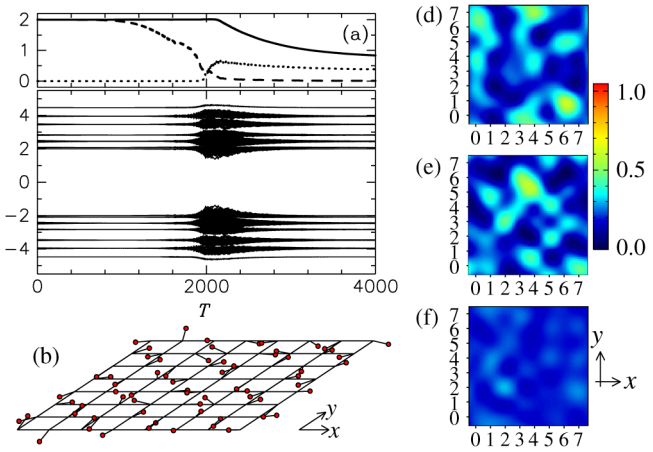

FIG. 3 (color online). Time evolution of the double-exchange model. The parameter set, $t = 1$, $SJ_H = 2$, $S\alpha = 0.01$, $S = 1$, $\Delta T = 0.008$, is used. (a) The same with Fig. 1(a). (b) Structure of local spins at $T = 2000$. Distribution of energy density at (d) $T = 2000$, (e) $T = 2100$, and (f) $T = 2200$.

mechanism of the quantum transitions in generic interacting electron systems.

With further time evolution in stage (I), the energy level structure becomes disordered reflecting the disordered spin configuration, and the spectral density does not show characteristic frequency in this case [see Fig. 2(f)] since it is given by many components corresponding to various $\varepsilon_n - \varepsilon_m$.

Figure 2(c) shows the motion of the local spin marked by an ellipse in Fig. 1(d) for stage (II). As seen in the inset of Fig. 2(c), the local spin shows a *rapid* precession. Figure 2(d) shows the electron occupation number at the lowest energy state (in-gap state) in the upper energy band. In this case, however, the Rabi-oscillation behavior has not been observed. This is because the excited electrons in the states forming the bottom of the upper energy band show a cascade relaxation process, and the several frequencies are involved in those [see Fig. 2(g)]. It is seen, in fact, that at the early period of stage (II), the excited electrons occupy the lowest energy states of the upper energy band, and from the those states an in-gap state appears (see Fig. 1). Corresponding to the differences between those energy levels, the spectral density in Fig. 2(g) has the peak around $\omega \cong 1$. In other words, the interband transition occurs successively through those energy levels. Therefore, the dynamics similar to the ESR process is also essential for the interband transition in this stage (II). In stage (III), there occurs no quantum transition any more because $\langle 1|\vec{\sigma}_i|2\rangle \times \vec{S}_i^{\text{slow}} = \vec{0}$ for the AFM state.

The time scale for the *slow* motion of the local-spin dynamics is determined by the driving force from the excited electrons, and is estimated as $2\pi/\{n_{\text{ex},i} J_H S\alpha/[1 + (S\alpha)^2]\}$, where $n_{\text{ex},i}$ is the local density of the excited electrons at site i. Roughly speaking, $n_{\text{ex},i}$ is estimated to be $1/N_{\text{eff}}$ where N_{eff} is the spatial extent of the wave functions of the excited states. Even when the wave function is localized almost in a single site as shown in Fig. 1(h), $n_{\text{ex},i}$ at that site is of the order of 0.2. Therefore, the time scale of the local-spin dynamics is of the order of $4\pi/0.2 \cong 60$ even for $S\alpha = 1$ in the unit of $(J_H)^{-1}$.

We have examined the relaxation dynamics for a large number of numerical conditions, i.e., the parameter sets, the initial spin configurations, and the system sizes (up to 12×12 system). Although the specific pattern depends on the numerical conditions, the qualitative behavior of the relaxation dynamics is essentially insensitive to them.

We have also studied the more realistic case of $S\alpha = 0.01$ (Fig. 3). The mechanism of the relaxation dynamics for $S\alpha = 0.01$ is essentially the same with the previous case. For small $S\alpha$, a large number of local spins show very active dynamics. As a result, the relaxation process is accelerated, and the 10 times difference in the *slow* time scale appears although a hundred times difference in the magnitude of $S\alpha$ is in this case (see Figs. 1 and 3).

In summary, we have studied the real-time relaxation dynamics of the electron-spin coupled systems. The nanoscale structure of quantum origin observed in our calculation is expected to be ubiquitous to relaxations in interacting electronic systems.

The authors are grateful to Y. Tokura, M. Kawasaki, H. Matsueda, T. Tohyama, S. Ishihara, and K. Tsutsui for useful discussions. This work is supported by a Grant-in-Aid for Scientific Research (Grants No. 19048015, No. 19048008, No. 17105002, No. 21244053, No. 18560043, No. 19014017, No. 19204035, and No. 21360043) and a High-Tech Research Center project for private universities from the MEXT of Japan, Next Generation Supercomputing Project of Nanoscience Program, JST-CREST, and NEDO.

[1] M. Imada, A. Fujimori, and Y. Tokura, Rev. Mod. Phys. **70**, 1039 (1998).
[2] E. Dagotto, Science **309**, 257 (2005).
[3] Y. Ogawa *et al.*, Phys. Rev. Lett. **84**, 3181 (2000).
[4] Y. Mitsumori *et al.*, Phys. Rev. B **69**, 033203 (2004).
[5] S. Koshihara *et al.*, Phys. Rev. Lett. **78**, 4617 (1997).
[6] K. Miyano *et al.*, Phys. Rev. Lett. **78**, 4257 (1997).
[7] M. Fiebig *et al.*, Science **280**, 1925 (1998).
[8] P. W. Anderson, *Basic Notions of Condensed Matter Physics*, Advanced Book Program (Benjamin/Cummings Publishing Company, Inc., Menlo Park, California, 1984).
[9] H. Matsueda and S. Ishihara, J. Phys. Soc. Jpn. **76**, 083703 (2007).
[10] H. Matsueda *et al.*, Phys. Rev. B **77**, 193112 (2008).
[11] K. Yonemitsu and N. Maeshima, Phys. Rev. B **79**, 125118 (2009).
[12] P.-G. de Gennes, Phys. Rev. **118**, 141 (1960).
[13] M. Imada and Y. Hatsugai, J. Phys. Soc. Jpn. **58**, 3752 (1989).
[14] For the Fourier analysis, 2^{12} points with a small time increment $\Delta T = 0.008$ in units of $1/t$ are used.